Upper limits of dielectric permittivity modulation in bacteriorhodopsin films

P. Acebal, S. Blaya, L. Carretero, and A. Fimia*
Departamento de Ciencia y Tecnología de Materiales, Universidad Miguel Hernández, Av. Ferrocarril s/n Apdo, 03202 Ed. Torrevaillo, Elx (Alicante), Spain
(Received 25 May 2004; revised manuscript received 9 November 2004; published 19 July 2005)

A theoretical study of light-induced modulation of the dielectric permittivity in bacteriorhodopsin films has been done (including $B \rightarrow M$ and $B \rightarrow Q$ transitions). Analysis of dielectric permittivity modulation enables us to determine the fundamental limits of BR to be used in a holographic data storage system, together with the optimum experimental and material conditions. In order to carry out this analysis, the macroscopic dielectric permittivity was related to the microscopic polarizability of the three states of BR considered (B, M and Q). This parameter was calculated using a modelization procedure that includes the effect of ASP85, TRP86, and TYR185 aminoacid residues (the B3LYP/6-31+G* method was used for the calculations). Good concordance between theoretical calculations and experimental data was found for the linear optical properties (absorption wavelength, transition dipole moment, and dielectric permittivity modulation). The theoretical upper limits of $\Delta\epsilon$ at 750 nm (far from the resonance of the molecule) in a randomly oriented material are about 0.01 and 0.012 for $B \rightarrow M$ and $B \rightarrow Q$ transitions, respectively. The values of $\Delta\epsilon$ obtained were used to simulate diffraction efficiencies (η) of a volume phase hologram recorded in a BR film. The high absorptive losses at low wavelengths (about 625 nm) cause an interesting behavior, since the highest $\Delta\epsilon$ do not produce the greatest η. The highest η is produced for a hologram thickness in the range of 900–1000 μm and working wavelength of 700–750 nm.

DOI: 10.1103/PhysRevE.72.011909 PACS number(s): 87.15.Aa, 87.15.He, 78.20.Ci, 42.70.Ln

I. INTRODUCTION

Holographic recording materials have attracted a great deal of research activity in recent years due to their important applications, such us holographic interferometry, image processing or optical data storage [1,2]. In particular, materials for holographic data storage are in great demand in order to achieve high storage densities and fast access times [3]. Great advances have been made with write once-read many materials, like photopolymers or photo-addressable mixtures [3], and some are now commercially available. This is not the case of materials with the capacity to be erased and rewritten, since important work still needs to be done on these. Photochromic retinal protein bacteriorhodopsin (BR), which is contained within the purple membrane (PM) of members of the *halophilic archaea* species, is a promising material [4–8], since it supports a large number of write-erasure cycles.

Two different frames may be distinguished in the BR molecule. On the one hand, a chain of aminoacids forms a helicoidal superstructure shown in Fig. 1, whose main function is to serve as a rigid support for the light active core inside the bacterial membrane. This core is composed of a few aminoacids and the retinal chromophore attached to the lysine 216 via protonated Schiff base linkage (PSBR). The function of this active core is to act as light-driven proton pump, transforming light energy into chemical energy by a mechanism which has been described previously [5,9], with a high quantum efficiency. This mechanism is composed of six states (see Fig. 1). Regarding the optical properties, only the two states that involve the most stable structures of retinal-lys216 chromophore may be considered. These states are the initial B state (all-trans protonated isomer of retinal, Fig. 1), which upon illumination is converted into the M state (deprotonated C13 cis isomer of retinal, figure 1) via K and L states, returning to the B state via N and O states. Another photocycle was discovered in BR by Popp *et al.* [10] (denoted by dashed lines in Fig. 1). This second photocycle, also related to the retinal chromophore, starts at the O state, which upon red illumination is converted into the P state (C9 cis isomer of retinal). This P state is thermally unstable, and in the presence of water a hydrolyzed retinal molecule is formed, the so-called Q state (C9 cis isomer of hydrolyzed retinal, Fig. 1), which upon blue illumination returns to the B state.

Two basic requirements must be met in order to employ a photochromic molecule as a stable holographic recording material. First, it has to be bistable, with a long lifetime in both states. In BR, the M state lifetime has a wide range of values, depending on the genetic variation considered [9], but it also needs to be optimized, while the Q state has a long lifetime [11] (7–12 years at ambient temperature). The second requirement is to have high diffraction efficiencies (this implies large storage capacity) outside the absorption wavelength, which enables reading without erasure. Kogelnik's theory [12] shows that the diffraction efficiency of a phase volume grating depends on the hologram thickness and the modulation of the real part of the dielectric permittivity of the medium between the illuminated and nonilluminated zones. Therefore, theoretical analysis of dielectric permittivity modulation enables us to determine the fundamental limits of BR to be used in a holographic data storage system, together with the optimum experimental and material conditions. In order to carry out this analysis, the dielectric per-

*Electronic address: pablo@dite.umh.es

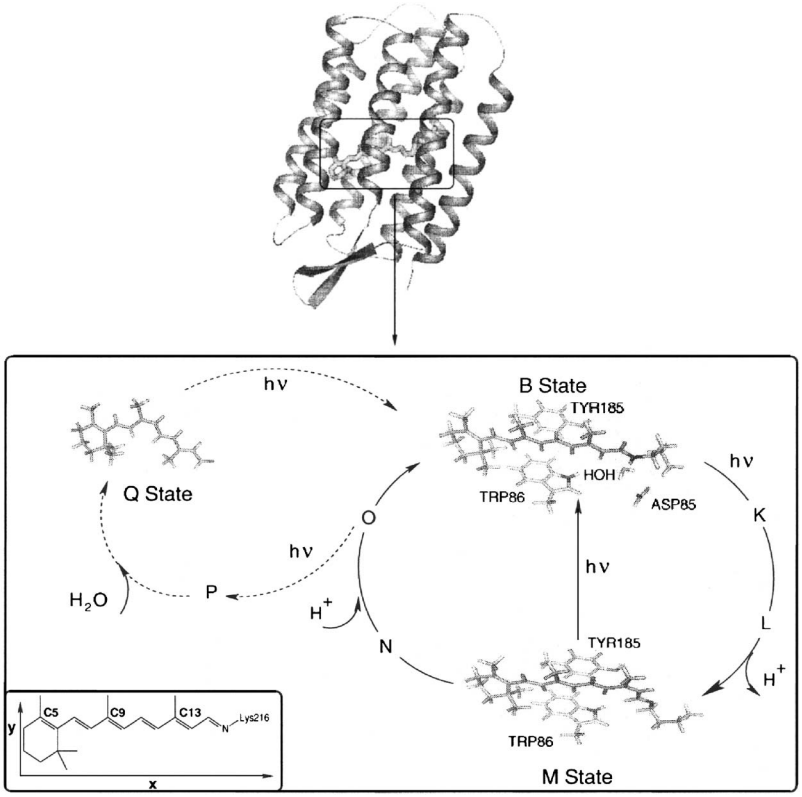

FIG. 1. Schematic representation of the bacteriorhodopsin structure and its photocycles.

mittivity of illuminated and nonilluminated zones was related to the microscopic polarizability of the different states. The frequency dependent polarizability of each state was calculated with a density functional method using an approximation of the sum over states expression [13].

II. THEORETICAL BACKGROUND

Dielectric permittivity (ϵ) is related to macroscopic optical susceptibility (χ) by $\epsilon_{ij}=1+\chi_{ij}$, therefore knowledge of χ_{ij} of the different states is the key to determining the ϵ modulation. Macroscopic optical susceptibility can be expressed as a function of the microscopic properties of the different elements of the system. In the case of BR, we considered the optical susceptibility to be made up of two contributions

$$\chi_{II}(\omega;\omega) = \chi_{II,prm}(0) + \chi_{II,ret}(\omega;\omega). \tag{1}$$

On the one hand, the contribution of the matrix (when it is dispersed in a polymer or a solvent) and the aminoacid superstructure is present in the first term of Eq. (1) $[\chi_{II,prm}(0)]$. The zero denotes that it is independent of the electromagnetic field frequency for the range considered (visible light), since it is far from the resonance for this part of the material. We also considered that this contribution does not change for the different states of the material, so it has no influence on the ϵ modulation. On the other hand, we considered the contribution of the light active core $[\chi_{II,ret}(\omega;\omega)]$, which was related to the microscopic properties of the retinal-lys216 molecule by the equation

$$\chi_{II,ret}(\omega;\omega) = \sum_s N^s \sum_i \zeta_i f(\omega)^2 \alpha_{ii}^s(\omega;\omega), \tag{2}$$

where N^s is the density of molecules in the s state, $\alpha_{ii}^s(\omega;\omega)$ is the s state polarizability, $f(\omega)$ is the local field factor [14] and ζ_i is a function related to the orientational average of the chromophores (I and i denote the macroscopic and microscopic frames, respectively). It is important to note that the main axes selected for both frames were eigenvectors of the optical properties, which implies that the off-diagonal terms are not considered. The bottom-left corner of Fig. 1 shows the coordinates system of the microscopic frame. The x direction is defined along the double bond structure of retinal. This structure forms the xy plane, with the z direction being perpendicular to the scheme. The ζ_i values depend on the order of the molecules. When $i \equiv I$, ζ_i changes between 1/3 for a randomly oriented material and 1 for a totally oriented material, while when $i \neq I$, ζ_i varies from 1/3 for a randomly oriented material to 0 for a totally oriented material.

Therefore, for the steady state of the grating formation, the BR optical susceptibilities in the illuminated $[\chi_{II}(\omega;\omega)^{b,ph}]$ and nonilluminated $[\chi_{II}(\omega;\omega)^a]$ zones are given by the equation

$$\chi_{II}(\omega;\omega)^a = \chi_{II,prm}(0) + N\sum_i \zeta_i \alpha_{ii}^{\beta}(\omega;\omega) f(\omega)^2, \tag{3}$$

$$\chi_{II}(\omega;\omega)^{b,ph} = \chi_{II,prm}(0) + N^B \sum_i \zeta_i \alpha_{ii}^B(\omega;\omega) f(\omega)^2 + N^{ph} \sum_i \zeta_i \alpha_{ii}^{ph}(\omega;\omega) f(\omega)^2, \tag{4}$$

where N is the total density of retinal molecules and the

superscript ph indicates the photocycle considered (M or Q). The difference between Eqs. (4) and (3) gives the final expression for the dielectric permittivity modulation:

$$\Delta\epsilon_{II}^{ph}(\omega;\omega) = \Delta\chi_{II}^{ph}(\omega;\omega) = N\phi^{ph}f(\omega)^2\sum_i \zeta_i(\alpha_{ii}^{ph}(\omega;\omega) - \alpha_{ii}^{\beta}(\omega;\omega)), \quad (5)$$

where we have defined the efficiency of conversion ($\phi^{ph} = N^{ph}/N$) from the initial B state to the other stable state of the photocycle (M or Q).

A. Microscopic polarizability

Perturbation theory provides an expression for the frequency dependent polarizability consisting of the sum of contributions from all the possible electronic states of the system [13] (sum over states). Therefore, the polarizability tensor components are given by the equation

$$\alpha_{ii}(\omega;\omega) = \sum_e \alpha_{ii,e}(0)\Omega_e(\omega;\omega), \quad (6)$$

where the contribution of each electronic state is written as a product of a static part $[\alpha_{ii,e}(0)]$, without frequency dependency, and a dispersion function $[\Omega_e(\omega;\omega)]$. In the case of BR, we considered that the frequency dependency in the range of visible light is only due to the first excited state, since the resonance frequencies of the other excited states are far from the frequencies of interest, so $\alpha_{ii}(\omega;\omega)$ can be written as

$$\alpha_{ii}(\omega;\omega) \approx \sum_{e,e\neq 1} \alpha_{ii,e}(0) + \alpha_{ii,1}(0)\Omega_1(\omega;\omega). \quad (7)$$

The static part and the dispersion function are given by the following equations [13]:

$$\alpha_{ii,e}(0) = \frac{2\mu_{ge,i}^2}{\hbar\epsilon_0\omega_{ge}}, \quad (8)$$

$$\mu_{ge,i} = \int_V \rho_{ge} r_i dv, \quad (9)$$

$$\Omega_1(\omega;\omega) = \frac{\omega^2}{\omega_{g1}^2 - \omega^2}, \quad (10)$$

where $\mu_{ge,i}$ is the i component of transition dipole moment between the ground and e excited state, r_i is the i component of the spatial coordinate, $\hbar$ is the Planck constant divided by 2π, ϵ_0 is the dielectric permittivity of a vacuum, and ω_{ge} is the resonance frequency between the ground and e excited state. In Eq. (9) ρ_{ge} is the transition density between the ground and e excited state, which is defined as the product of the wave functions of both states ($\Psi_g^*\Psi_e$).

III. MODELIZATION OF LIGHT ACTIVE CORE

Theoretical evaluation of the microscopic optical properties of BR is a difficult task, since the medium surrounding PSBR produce significant changes in these properties as compared to those of the isolated chromophore in solution. For example, the absorption maximum of the B state is redshifted about 0.6 eV from that of PSBR chloride in methanol [4]. This shift, the so-called opsin shift, is explained by various mechanisms, which are (i) the change in the π-bond distribution between the C5-C6 cis isomer of PSBR present in solution and the C5-C6 trans isomer of the protein [15,16]; (ii) the weakening of the interaction between PSBR and its counterion [17,18]; (iii) and the interaction of PSBR with polarizable aminoacids of the protein [17,18]. This section described the procedure employed to calculate the microscopic properties of B and M states of BR taking into account the environmental effect.

A. *B* state

A schematic representation of the procedure employed to calculate the optical properties is shown in Fig. 2. Two strategies were used for the two different mechanism previously described that cause the opsin shift. On the one hand, the effect of the counterion was studied including in the calculations the ASP85 residue ($HCOO^-$; see Fig. 1), which is the nearest negatively charged aminoacid to the protonated Schiff base linkage, and a water molecule, which according to the semiempirical study of Kutnerzow *et al.* has an influence on the weakening of the interaction [19]. The position of the ASP85 residue with respect to PSBR (the geometry was previously optimized with HF/6-31G) was fixed using experimental crystallographic data from the Protein Data Bank [20]. The relative position of the water molecule was determined with a semiempirical AM1 calculation, where the coordinates of PSBR and ASP85 residues remain constant. On the other hand, to study the effect of polarizable aminoacids, we included the electrostatic interactions with TRP86 (indole) and TYR185 (phenol) residues, which are the nearest residues to PSBR, and according to a previous study of Houjou *et al.* play a predominant role in the bathochromic shift in the absorption band [18]. To do this, Mulliken charges of TRP86 and TYR185 residues located at experimental crystallographic coordinates [20] were included in the calculations of the microscopic optical properties. Since PSBR-ASP85-H_2O is a highly dipolar system and both residues are also highly polarizable, in the calculation of the Mulliken charges we also included the electric field caused by PSBR-ASP85-H_2O dipole moment at TRP86 and TYR185 locations.

Mulliken charges and the microscopic optical properties were simulated with a density functional method (DFT), which has been shown to be a good approximation in the study of the optical properties of molecules [21–23]. The method selected is Becke's three parameter mixing of exchange and Lee-Yang-Parr's correlation functionals (known as B3LYP) [24] with the 6-31+G* basis set. Two techniques were used in the calculation, depending on the properties calculated. Static polarizability was calculated with the finite field technique [25]. The contribution of the first excited state was calculated with Eqs. (8) and (10), where $\mu_{ge,i}$ and ω_{ge} were evaluated using time-dependant DFT (TDDFT). In or-

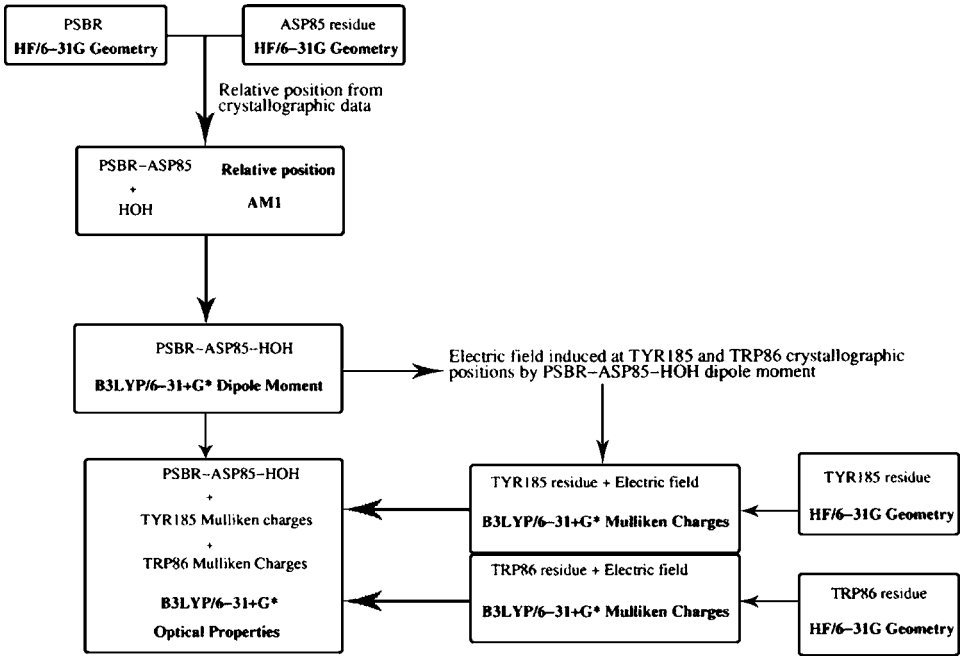

FIG. 2. Schematic representation of the procedure used to calculate the optical properties.

der to take into account the zero-point energy of the quantum harmonic oscillator [26], the values calculated for electronic transitions, which correspond to the vertical absorption energy, have to be corrected by the zero-point vibrational energy difference between the ground and excited states ($\Delta E_{ZP}=E_{ZPe}-E_{ZPg}$). We use a $\Delta E_{ZP}=-0.15$ eV to correct the values obtained in all cases. To evaluate the contribution of the interaction with the polarizable aminoacids TRP86 and TYR185 in the opsin shift, we also calculated the absorption wavelength without including the charges of both aminoacids.

B. *M* state

Since the *M* state is a unprotonated isomer of Schiff base retinal (SBR), no influence of the counterion may be expected, so we do not include ASP85 or the water molecule in the calculations. The influence of TRP86 and TYR185 residues was evaluated with the same procedure as for the *B* state (experimental crystallographic positions from protein Data Bank [27]). During HF/6-31G geometry optimization, in order to finish at the 13-cis isomer of SBR all the dihedral angles between C5 and C13 were fixed at the values of the all-trans isomer.

C. *Q* state

The *Q* state is a free isomer of retinal (without linkage to the protein), and no effect of the environment was taken into account in the calculations due to the free rotation, which does not allow us to know the locations of the aminoacid residues with respect to the chromophore. As in the *M*-state geometry optimization, all the dihedral angles between C5 and C9 for the *Q* state were fixed at the values of the all-trans isomer (PSBR).

All the calculations of the microscopic properties of the chromophore were performed with the Gaussian 98 package [28].

IV. RESULTS AND DISCUSSION

Before giving a complete description of the calculated microscopic optical properties it is important to confirm that the modelization procedure employed in the calculations is correct. For this purpose, theoretical results of absorption wavelength and transition dipole moment of the three states were compared with experimental values (Table I). Especially noticeable is the good agreement between the calculated value for the *B* state and experimental data. This confirms that the modelization procedure explains the opsin shift correctly. Calculations also permit the contributions of the counterion and the polarizable aminoacids to the opsin shift to be estimated. As mentioned above, this shift is caused by three main contributions. The first contribution is the change in the π-bond distribution between the C5-C6 cis isomer of PSBR present in solution and the C5-C6 trans isomer of the protein, to which we assigned a total weight of 0.22 eV using the experimental data in Ref. [29]. Therefore, the other 0.38 eV needs to be justified by the other two mechanisms (effect of the counterion and polarizable aminoacids). The results obtained with (PSBR-ASP-H_2O) and without (*B* state) the charges of the polarizable aminoacids TRP86 and TYR185 suggest that the weight of these aminoacids is approximately 0.17 eV (the large polarization of these aminoacids with the ion-pair PSBR-ASP85 is important for this contribution), so about 0.21 eV could be assigned to the weakening of the interaction between the PSBR and its counterion. These results are of the same order of magnitude as those of previous studies by Houjou *et al.* using semiempirical methods [17], that attribute about 0.15 eV to the counterion interaction and 0.12 eV to the medium. Therefore, our calculations suggest that the three mechanisms play an important role in the opsin shift. For the other two states good concordance between calculated values and experimental data is also obtained, especially for the *M* state, while experimental *Q* state absorption is blue shifted around 0.26 eV

TABLE I. Calculated values for the absorption energies E_{eg} [in parenthesis the correspondence in wavelength (nm)] and transition dipole moment using the B3LYP/6-31+G* method and the procedure previously described.

		B state	PSBR-ASP-H_2O	*M* state	*Q* state
E_{eg} (eV)	Calc.	2.219 (*559*)	2.387 (*519*)	2.99 (*414*)	2.917 (*425*)
	Expt.	2.183 (*568*[a])		3.0 (*412*[a])	3.179 (*390*[b])
μ_{ge} (10^{-29} Cm)	Calc.	4.42	4.37	3.69	3.03
	Expt.	3.75[a]		2.95[a]	2.79[b]

[a]From Ref. 30.
[b]Estimated from the experimental curves in Ref. 11.

with respect to the calculated value. Regarding transition dipole moment values, also a good concordance with experimental values is also obtained. In the three cases, the calculated values are greater than the experimental ones, but with small differences (the relative errors are 18%, 25%, and 8% for *B*, *M*, and *Q* states, respectively). Therefore, the modelization procedure proposed could be considered a good alternative to simulate the optical properties of bacteriorhodopsin.

Table II shows the main results obtained from the calculations done for polarizability of the three BR states. As may be expected, the greatest component of static polarizability is the $\alpha_{xx}(0)$, which is the direction with a large extent of conjugation of π bonds. The other component of the molecular plane [$\alpha_{yy}(0)$] is about 5 times smaller than $\alpha_{xx}(0)$ for the *B* state and about 2 times smaller for the other two states. This different relation may be explained by the increase in the π electron conjugation along the *y* direction for the 9-cis and 13-cis isomers of retinal. Comparison of the different states shows that the change of static polarizability is greater for the $\alpha_{xx}(0)$ component (about 9×10^{-28} m^3 and 10^{-27} m^3 for $B\rightarrow M$ and $B\rightarrow Q$ transitions, respectively), while the differences between the other two components of the main diagonal are small (less than 1.4×10^{-28} m^3 for both photocycles). Therefore, the susceptibility modulation will be mainly due to one microscopic component ($\Delta\alpha_{xx}$), so large changes in $\Delta\chi$ between totally oriented and randomly oriented material may be expected.

So far we have discussed the static linear optical properties of retinal in the different states, but no frequency dependency has been dealt with. With the approximations described in the theoretical background, the frequency dependency is given only by the dispersion function of the first excited state [Eq. (10)] and the static polarizability due to this transition, so $\alpha_{xx,1}(0)$ was calculated. Regarding the static contribution of the first excited state, only the $\alpha_{xx,1}(0)$ component is not negligible. This could be explained by the transition densities between the ground and first excited state (ρ_{g1}), which are shown in Fig. 3 for the three states. These ρ_{g1} are mainly distributed along the chain of conjugated π bonds in all the cases, which implies that the volumetric integral of ρ_{g1} weighted by the spatial coordinate [Eq. (9)] only has a nonvanishing value for $\mu_{ge,x}$, as shown by the ratios $\mu^B_{ge,x}/\mu^B_{ge,y}=11.5$, $\mu^M_{ge,x}/\mu^M_{ge,y}=10.7$ and $\mu^Q_{ge,x}/\mu^Q_{ge,y}=8$ for the calculations, and so only the contribution of $\alpha_{xx,1}(0)$ is obtained. Calculated values of $\alpha_{xx,1}(0)$ can be seen in Table II. The weight of this state in the total $\alpha_{xx}(0)$ is approximately 50% of the total static value. This ratio is increased when we compare the change in the static polarizability of transitions $B\rightarrow M$ and $B\rightarrow Q$, since 80% of these changes is due to $\alpha_{xx,1}(0)$. Therefore, theoretical calculations show that the polarizability modulation is mainly due to the first excited state, which is in concordance with previous studies [31,32] that employ the experimental absorption spectra of the first excited state to obtain the real part of the refractive index modulation using the Kramers-Kronig relation.

TABLE II. Calculated values for the microscopic optical properties using the B3LYP/6-31+G* method and the procedure previously described.

	B	*M*	*Q*
$\alpha_{xx}(0)$ (10^{-28} m^3)	20.46	12.88	10.61
$\alpha_{yy}(0)$ (10^{-28} m^3)	5.87	5.59	4.40
$\alpha_{zz}(0)$ (10^{-28} m^3)	4.35	3.78	2.92
$\alpha_{xx,1}(0)$ (10^{-28} m^3)	12.28	6.37	4.55

The next step is to introduce the values of the microscopic properties into the model [Eq. (5)] to obtain the dielectric permittivity modulation. Before analyzing the $\Delta\epsilon$ upper limits, the feasibility of the model could be examined comparing the theoretical predictions with experimental data for the $B\rightarrow M$ transition obtained from a previous experimental study [33]. For this purpose, we employ the following experimental measurement conditions: $\lambda=633$ nm, $N=8.77\times10^{23}$ molecules/m^3 (using a molecular weight of 26000 Dalton) and $\phi^M=0.363$ (obtained from transmittance variation curves of Ref. [33]), $f(\omega)=1.32$ (using a refractive index of 1.4) and $\zeta_i=1/3$ (randomly oriented material). The theoretical prediction of $\Delta\epsilon$ with these conditions is 8.6×10^{-4}. There is good agreement between this result and the experimental value, which is $\Delta\epsilon_{exp}=6\times10^{-4}$ [33] [we used the relation $\Delta\epsilon=2\epsilon_1$ between the definition of the dielectric permittivity modulation in the Kogelnik's theory [12] (ϵ_1) and our definition of the dielectric permittivity modulation ($\Delta\epsilon$)], where we considered that the phase grating is recorded over all the thickness of the film (330×10^{-6} m). The difference between experimental data and theoretical calculations could be smaller, because due to the high absorption

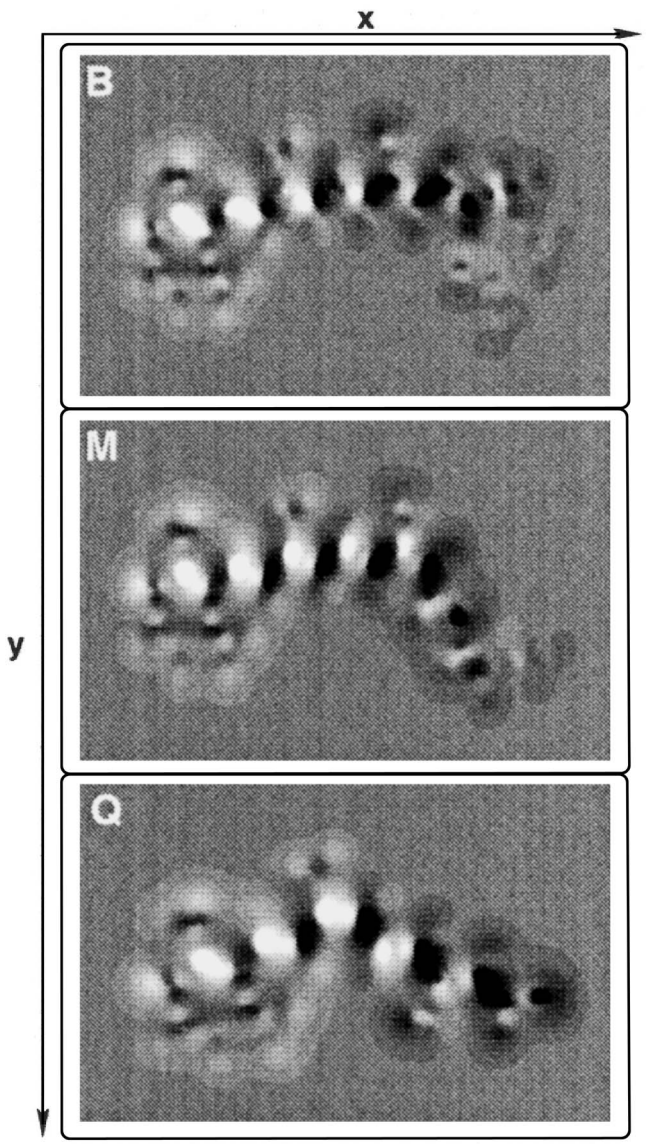

FIG. 3. Projection onto the *xy* plane of the transition densities between ground and first excited state calculated with the B3LYP/6-31+G* method (white and black colors denote positive and negative values, respectively).

of the material, it is reasonable to think that the effective thickness of the hologram is less, so a higher effective $\Delta\epsilon_{exp}$ will be expected (for example, if the effective thickness of the material was 75% of the real thickness the experimental value would be $\Delta\epsilon_{exp}=8\times10^{-4}$).

Since good agreement is encountered between experimental and theoretical data, microscopic optical properties could be used to determine the theoretical upper limits of $\Delta\epsilon$ for both photocycles of bacteriorhodopsin. To do this, ideal values of the other parameters in equation 5 may be used. This implies the employment of maximum values for conversion efficiency for this system ($\phi=0.65$) and density of chromophores ($N=1/\text{volume}_{BR}\approx10^{25}$). The evolution of the main component of the $\Delta\epsilon$ with the working wavelength for both photocycles is shown in Fig. 4. In the simulations three different degrees of order were used (randomly oriented material $\zeta_i=1/3$, moderately oriented material $\zeta_i=2/3$ and totally oriented material $\zeta_i=1$). As was mentioned above, a strong influence of the order of the system on the maximum $\Delta\epsilon$ is found, since an increase in the degree of order causes it to increase by a factor of 3 and the values of the other two components to decrease to zero. For the randomly oriented case, the $B\rightarrow M$ transition has a theoretical upper limit of $\Delta\epsilon\approx0.014$ at 650 nm, which is two orders of magnitude greater than that obtained experimentally, so the material's behavior will still need to be optimized. This optimization will involve a change in the environment to increase the conversion efficiency and also an increase in the density of molecules. The use of an ordered system will also increase the $\Delta\epsilon$ by a factor of 3, which allows us to obtain $\Delta\epsilon_{xx}\approx0.02$ at a wavelength as high as 800 nm, very far from the resonance of the retinal chromophore, which is necessary to read without erasure and to minimize the absorptive losses. All the curves have a asymthotic behavior to long wavelengths, with the cutoff values being proportional to the difference in the static polarizabilities $[\alpha(0)]$ between the states considered. Regarding the $B\rightarrow Q$ transition, greater modulations than in the M state photocycle were obtained throughout the range of the spectrum, with values of about 0.042 at 650 nm for a totally oriented system. Since the $B\rightarrow Q$ transition has the highest ϵ modulation and the longest stability, it will be a better candidate than the $B\rightarrow M$ transition for use in a holographic data storage system, but the conversion efficiency of both photocycles must also be taken into account.

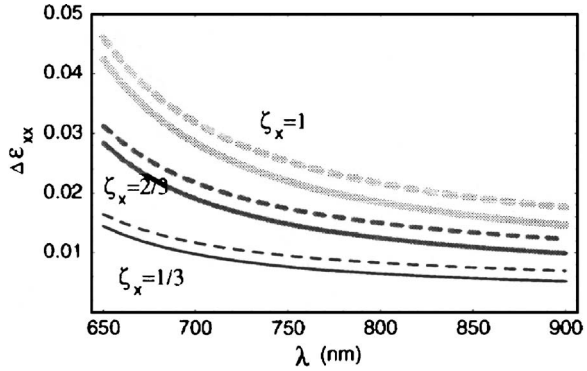

FIG. 4. Theoretical upper limits of the dielectric permittivity modulation of BR for $B\rightarrow M$ (black lines) and $B\rightarrow Q$ (dashed lines) transitions versus the working wavelength ($\phi=0.65, N=10^{25}$).

A. Diffraction efficiency

As mentioned in the Introduction, stable holographic data storage material requires high storage capacity. The diffraction efficiency (η) of a holographic grating will be a first approximation to the material's storage capacity and is also important for other holographic applications. This η for a volume phase grating is given by Kogelnik's expression [12]:

$$\eta=\exp\left[\frac{-2A}{\cos\theta}\right]\sin^2\left(\frac{\pi d\epsilon_1(\omega;\omega)}{2n\lambda\cos\theta}\right), \tag{11}$$

where d is the hologram thickness, θ is the Bragg angle of the grating for a given λ, n the refractive index, A is the

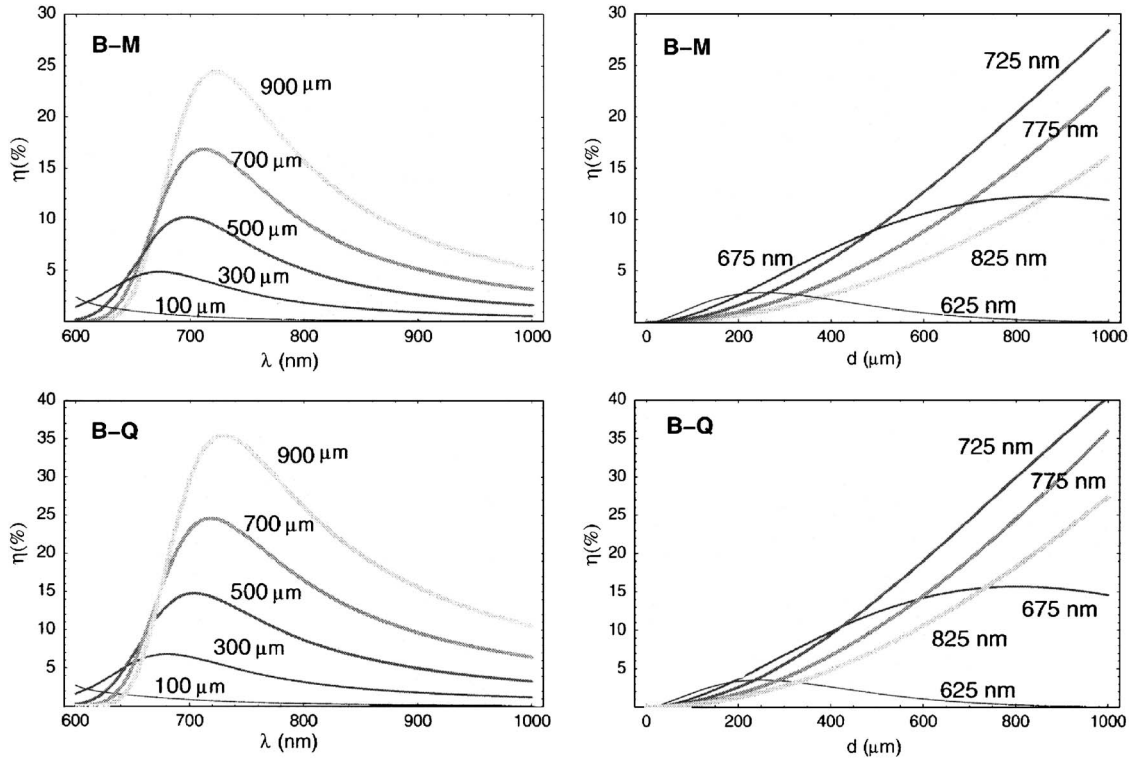

FIG. 5. Simulations of diffraction efficiency (η) for $B \rightarrow M$ and $B \rightarrow Q$ transitions of BR versus the reading wavelength (λ) for various hologram thicknesses (left part, gray level and line thickness increases with d) and the hologram thickness (d) for various λ (right part, gray level and line thickness increases with λ). The values of the other variables used are $\zeta_i = 1/3$, $N = 8.77 \times 10^{23}$ molecules/m^3, $\phi = 0.65$, B3LYP/6-31+G* values of microscopic properties and $\theta = 13.8$, which was the same as in the experimental setup of Ref. [33].

absorption of the film at the reading wavelength and $\epsilon_1(\omega;\omega) = \Delta\epsilon/2$. Since the working wavelengths are in the range of 650 to 900 nm, the film absorption after exposure may be considered to be only due to the B state, which implies that the grating absorption could be expressed as $A \approx A_B(2-\phi)/2$. According to the experimental data [11], the theoretical absorption spectra of the B state was approximated to a normal distribution curve, centered in the calculated ω_{eg} and with a standard deviation of 50 nm (full width at half maximum $\approx$120 nm):

$$A_B = dC\kappa_B \frac{\exp\left[-\dfrac{(\omega-\omega_{eg})^2}{2\sigma}\right]}{(2\pi)^{1/2}\sigma}, \tag{12}$$

where σ is the standard deviation of the curve (in s^{-1}), C is the concentration (in molar units), and κ_B is the maximum molar absorptivity (in M^{-1} cm^{-1}) obtained from the equation

$$\kappa_B = \frac{2m_e\omega\mu_{eg}^2}{3e^2\hbar 1.44 \times 10^{-19}}, \tag{13}$$

where m_e and e are the electron mass and the electron charge, respectively.

Introducing in Eq. (11) the calculated $\Delta\epsilon(\omega;\omega)$ for both photocycles of BR, the diffraction efficiency can be simulated. These simulations are shown in Fig. 5, where we used the same angle as that in Ref. [33] ($\theta = 13.8$) and realistic values of the other variables ($\zeta_i = 1/3$, $N = 8.77 \times 10^{23}$ molecules/m^3, $n = 1.54$, and $\phi = 0.65$).

Diffraction efficiency for a volume phase hologram recorded in BR films is greatly influenced by the absorptive losses, so for a working wavelength of about 650 nm the simulated η value is lower than 5% for all the hologram thicknesses considered. This causes an interesting behavior, since the highest $\Delta\epsilon$ do not produce the greatest η. As can be seen in these curves, the highest values of η are obtained if the working wavelength is far from the resonance of the B state ($\eta \approx 25\%$ at 725 nm for $d = 900$ μm). These simulations estimate diffraction efficiencies greater than that of the largest experimental values found in the bibliography, and some comments are needed to explain these differences. An overestimation of η could be attributed to the ϕ value used, but this is not the key parameter in the large values obtained. The parameter that explains this behavior is the thickness of the hologram. Usually the films used for experimental measurements have a thickness of 100 μm or lower, and the working wavelength is about 633 nm. Under these conditions, the simulation values are about the same order of magnitude as the experimental values (lower than 5%), and η decreases with the increase in the working wavelength (note that only phase modulation was considered for simulations).

The optimum working wavelength for a given hologram thickness can be seen in the curves on the left in Fig. 5. This optimum λ increases when the film thickness is augmented, since it is about 680 nm for a hologram thickness of 300 μm

and about 720 nm for $d=700$ μm. The representation on the right in Fig. 5 enables us to evaluate the optimum hologram thickness for a given λ. As can be seen for the lower wavelengths, an overmodulation effect is encountered, and the optimum d is about 200 μm for 625 nm and 700 μm for 675 nm, while for the other λ used η increases with d in the range considered, so no overmodulation effect was obtained. It is also important to note that the hologram thickness must be greater than 100 μm in order to obtain significant diffraction efficiencies as phase material.

V. CONCLUSIONS

A theoretical study of light-induced modulation of the dielectric permittivity in bacterirhodopsin films has been done (including $B \rightarrow M$ and $B \rightarrow Q$ transitions). This macroscopic physical property was related to the microscopic polarizability of the three states of BR considered (B, M, and Q), and this parameter was calculated using a modelization procedure that includes the effect of ASP85, TRP86, and TYR185 aminoacid residues (the B3LYP/6-31+G* method was used for the calculations). Good concordance between theoretical calculations and experimental data was found for the linear optical properties (absorption wavelength, transition dipole moment and dielectric permittivity modulation). The main conclusions derived from the simulations are as follows.

Light-induced change in the chromophore's polarizability is mainly due to the contribution of the first excited state, since it accounts for about 80% of the static polarizability variation.

Only in the $\alpha_{xx}(\omega,\omega)$ component are there significant changes for $B \rightarrow M$ and $B \rightarrow Q$ transitions. This is explained by the transition density of the first excited state for the three BR states, which is distributed along the chain of conjugated π bonds (x direction). As a consequence, an increase in the dielectric permittivity modulation is obtained when the system's order is augmented.

The theoretical upper limits of $\Delta\epsilon$ at 750 nm (far from the resonance of the molecule) in a randomly oriented material are about 0.01 and 0.012 for $B \rightarrow M$ and $B \rightarrow Q$ transitions respectively. With the same conversion efficiency, the $B \rightarrow Q$ transition have higher values of $\Delta\epsilon$ than the $B \rightarrow M$ transition over all the spectrum studied.

The values of $\Delta\epsilon$ obtained was used to simulate diffraction efficiencies of a volume phase hologram recorded in a BR film. The high absorptive losses at low wavelengths (about 625 nm) cause an interesting behavior, since the highest $\Delta\epsilon$ do not produce the greatest η. The highest η is produced for a hologram thickness in the range of $(900-1000)\times10^{-6}$ m and a working wavelength of 700–750 nm. It is also important to note that the hologram thickness must be higher than 100 μm in order to obtain significant diffraction efficiencies as phase material. Estimated dynamic range ($M_{no.}$) for storage holograms with $\eta=0.1\%$ in a BR film of 900 μm and a working wavelength of 725 nm are 0.52 and 0.65 for the $B \rightarrow M$ and $B \rightarrow Q$ transitions, respectively.

ACKNOWLEDGMENTS

The authors acknowledge support from project MAT2004-04643-C03-03 and MAT2002-01690 of Ministerio de Ciencia y Tecnología of Spain.

[1] H. Coufal, Nature (London) **393**, 628 (1998).
[2] H. J. Coufal and G. T. Sincerbox, *Holographic Data Storage* (Springer, Berlin, 2000).
[3] J. Ashley, M.-P. Bernal, G. W. Burr, H. Coufal, H. Guenther, J. A. Hoffnagle, C. M. Jefferson, B. Marcus, R. M. Macfarlane, R. M. Shelby, and G. T. Sincerbox, IBM J. Res. Dev. **44**, 341 (2000).
[4] R. R. Birge, Annu. Rev. Phys. Chem. **41**, 683 (1990).
[5] N. Hampp, A. Popp, C. Bruchle, and D. Oesterhelt, J. Phys. Chem. **96**, 4679 (1992).
[6] A. Bablumian and T. Krile, Opt. Eng. (Bellingham) **39**, 2964 (2000).
[7] N. Hampp, Chem. Rev. (Washington, D.C.) **100**, 1755 (2000).
[8] J. A. Stuart, D. L. Marcy, K. J. Wise, and R. R. Birge, Synth. Met. **127**, 3 (2002).
[9] J. D. Downie and D. T. Smithey, Appl. Opt. **35**, 5780 (1996).
[10] A. Popp, M. Wolperdinger, N. Hampp, C. Brauchle, and D. Oesterhelt, Biophys. J. **65**, 1449 (1993).
[11] N. Gillespie, K. Wise, L. Ren, J. Stuart, D. Marcy, J. Hillebrecht, Q. Li, L. Ramos, K. Jordan, S. Fyvie, and R. R. Birge, J. Phys. Chem. B **106**, 13352 (2002).
[12] H. Kogelnik, Bell Syst. Tech. J. **48**, 2909 (1969).
[13] *Nonlinear Optical Materials. Theory and Modeling*, edited by S. P. Karna and A. T. Yeates (American Chemical Society, Washington, 1996).
[14] R. Wortmann and D. M. Bishop, J. Chem. Phys. **108**, 1001 (1998).
[15] R. van der Steen, P. L. Biesheuvel, R. A. Mathies, and J. Lugtenburg, J. Am. Chem. Soc. **108**, 6410 (1986).
[16] J. Lugtenburg, M. Muradin-Szweykowska, C. Heeremans, and J. A. Pardoen, J. Am. Chem. Soc. **108**, 3104 (1986).
[17] H. Houjou, Y. Inoue, and M. Sakurai, J. Am. Chem. Soc. **120**, 4459 (1998).
[18] H. Houjou, Y. Inoue, and M. Sakurai, J. Phys. Chem. B **105**, 867 (2001).
[19] A. Kusnetzow, D. L. Singh, C. H. Martin, I. J. Barani, and R. Birge, Biophys. J. **76**, 2370 (1999).
[20] Y. Matsui, K. S. M. Murakami, Y. Shiro, S. Adachi, H. Okumura, and T. Kouyama, J. Mol. Biol. **324**, 469 (2002).
[21] C. Adamo and V. Barone, Chem. Phys. Lett. **330**, 152 (2000).
[22] R. Pou-Amérigo, P. M. Viruela, R. Viruela, M. Rubio, and E. Ortí, Chem. Phys. Lett. **352**, 491 (2002).
[23] M. Parac and S. Grimme, Chem. Phys. **292**, 11 (2003).
[24] A. D. Becke, J. Chem. Phys. **98**, 5648 (1993).

[25] H. D. Cohen and C. C. J. Roothaan, J. Chem. Phys. **43**, S34 (1965).
[26] P. Acebal, S. Blaya, and L. Carretero, Chem. Phys. Lett. **374**, 206 (2003).
[27] H. J. Sass, J. Berendzen, D. Neff, R. Gessenich, P. Ormos, and G. Bueldt, Protein data bank (1999), http://www.rcsb.org/pdb/.
[28] M. J. Frisch, G. W. Trucks, H. B. Schlegel, G. E. Scuseria, M. A. Robb, J. R. Cheeseman, V. G. Zakrzewski, J. A. Montgomery, R. E. Stratmann, J. C. Burant, S. Dapprich, J. M. Millam, A. D. Daneils, K. N. Kudin, M. C. Strain, O. Farkas, J. Tomasi, V. Barone, M. Cossi, R. Cammi, B. Menucci, C. Pomelli, C. Adamo, S. Clifford, J. Ochterski, G. A. Petereson, P. Y. Ayala, Q Cui, K. Morokuma, D. K. Malick, A. D. Rabuck, K. Raghavachari, J. B. Foresman, J. Cioslowski, J. V. Ortiz, B. B. Stefanov, G. Liu, A. Liashenko, P. Piskorz, I. Komaromi, G. Gomperts, R. L. Martin, D. J. Fox, T. Keith, M. A. Al-Laham, C. Y. Peng, A. Nanayakkara, C. Gonzalez, M. Challacombe , P. M.W. Gill, B. G. Johnson, W. Chen, M. W. Wong, J. L. Andres, M. Head-Gordon, E. S. Replogle, and J. A. Pople, GAUSSIAN 98, Revision A.7, Gaussian, Inc, Pittsburg PA, 1998.
[29] A. Lewis, A. Khatchatouriants, M. Treinin, Z. Chen, G. Peleg, N. Friedman, O. Bouevitch, Z. Rothman, L. Loew, and M. Sheres, Chem. Phys. **245**, 133 (1999).
[30] J. Y. Huang, Z. Chen, and A. Lewis, J. Phys. Chem. **93**, 3314 (1989).
[31] D. A. Timucin and J. D. Downie, J. Opt. Soc. Am. B **14**, 3285 (1997).
[32] R. B. Gross, K. C. Izgi, and R. R. Birge, in *Image Storage and Retrieval Systems*, Proc. SPIE Vol. 1662 (SPIE, Bellingham, WA, 1992), pp. 186–196.
[33] A. Fimia, P. Acebal, A. Murciano, S. Blaya, L. Carretero, M. Ulibarrena, R. Aleman, M. Gomariz, and I. Meseguer, Opt. Express **11**, 3438 (2003).